MIT Open Access Articles

A New Algorithm to Classify the Homogeneity of ERS-2 Wave Mode SAR Imagette

A New Algorithm to Classify the Homogeneity of ERS-2 Wave Mode SAR Imagette

Guiting Song · Jagabandhu Panda · Yanhui Zhang ·
Haoliang Chen · K. Muni Krishna

Abstract A new classification parameter is developed using 1535 ERS-2 wave mode synthetic aperture radar (SAR) test imagettes to better differentiate homogeneous and inhomogeneous imagettes. The comparison between the new parameter (Min) and the previous one (*Inhomo*) (Schulz-Stellenfleth and Lehner, 2004) was done under varied threshold values of *Inhomo*. It is concluded that the performance of 'Min' is much better than '*Inhomo*' when applying to the 1535 test imagettes. Furthermore, both Min and *Inhomo* are applied to nearly 1 million imagettes collected for the period from 1 September 1998 to 30 November 2000. The comparisons of the global inhomogeneous distribution between 'Min' and 'Inhomo' reveal that both the areas and percentage of inhomogeneity calculated by 'Min' are larger than that calculated by '*Inhomo*'. By analyzing the low wind speed distribution of HOAPS data, we found that low wind speed over the ocean is one of the key reasons for the inhomogeneity of SAR imagettes.

Keywords Synthetic aperture radar imagette ·
Homogeneity · Classification algorithm

G. Song (✉)
Department of Marine Science, Zhejiang Ocean University,
18 Haiyuan Rd,
Zhoushan 316000, China
e-mail: guitingsong@zjou.edu.cn

J. Panda
School of Physical and Mathematical Sciences,
Nanyang Technological University,
Singapore, Singapore
e-mail: jagabandhu@gmail.com

Y. Zhang
College of Resources and Environment,
Shandong Agricultural University,
Tai'an, China
e-mail: zhangyh@sdau.edu.cn

Y. Zhang
Key Laboratory of Agricultural Environment,
Universities of Shandong,
Jinan, China

H. Chen
Singapore-MIT Alliance for Research and Technology,
Singapore, Singapore
e-mail: chenhaoliang@smart.mit.edu

K. M. Krishna
Department of Meteorology and Oceanography,
Andhra University,
Visakhapatnam, India
e-mail: munikrishnna@yahoo.co.in

Introduction

During the last three decades, several satellite missions have provided meteorological and oceanic data sets for research and operational purposes to the weather, ocean and climate communities. In future, it is expected that the planned satellite missions will result in a five order of magnitude increase in the volume of data available for use by the operational scientists and researchers all over the world (Marshall et al. 2009). These data sets would provide accuracies in predicting the weather events and is expected to improve the environmental prediction capability. Analyzing the satellite data for any weather event is not so simple, since it involves various technicalities. However, the scientists are continuously trying to make use of the satellite products in weather, ocean and climate studies (e. g. Mitra et al. 2013). For example, the satellite derived data sets have been used for the study of surface and upper-air characteristics (Panda and Giri 2012), near-surface wind driven features over ocean surface (Deb et al. 2009), heavy rainfall events (Deb et al. 2008), and also for the studies related to tropical cyclones (Panda et al. 2011; Deb et al. 2011; Jaishwal et al. 2012, 2013).

In view of the utility of satellite products, appropriate techniques need to be developed (e. g. Jaishwal et al. 2012) for deriving the environmental parameters (both ocean and atmosphere) from remotely sensed measurements by the environmental satellites. For example, it has been demonstrated earlier that the synthetic aperture radar (SAR) imagette can be used to derive wave parameters like significant wave height, wind speed and mean wave period (Schulz-Stellenfleth et al. 2007). The empirical algorithm developed by Schulz-Stellenfleth et al. (2007) was called CWAVE and the imagette is the only input data for CWAVE, so the homogeneity feature of the imagette has important effect on the result of the CWAVE. Several studies in past have also analyzed the feature of SAR imagettes (Hasselmann et al. 1985; Lyzenga et al. 1985; Alpers and Bruemmer 1994; Horstmann et al. 2003; Schulz-Stellenfleth and Lehner 2004). These studies reveal that several factors such as ice, atmospheric features like rain or biogenic surface film, oil slick, or ship wake could make the imagettes inhomogeneous and such inhomogeneous imagettes could not be applied into CWAVE to retrieve wave parameters. Therefore, a homogeneity test must be performed beforehand. In

view of this, an effort is made in the current study to improve the performance of CWAVE by developing a new classification parameter of the imagette for CWAVE. Further, significance of this new classification parameter is discussed over several regions of the world. The study mainly uses the European satellite (ERS-2) products for the classification of imagettes and developing the new algorithm for this purpose.

Data Used

Two types of data sets are used in this study. One is the wave mode ERS-2 SAR imagettes and the other one is the HOAPS (Hamburg Ocean Atmosphere Parameters and Fluxes from Satellite) wind speed data. The details of these data sets are described in this section along with their utility in relating to the present study.

Wave Mode ERS-2 Imagette

The imagettes used in this study is wave mode ERS-2 imagettes which is 10 by 5 km size acquired every 200 km along the satellite track. The C-band radar operates with vertical polarization in transmit and receives and provides a spatial resolution of about 10 m in azimuth direction and 20 m in range direction. The required SAR wave mode single look complex (SLC) imagettes, which are not available as standard products, were reprocessed at German Aerospace Center (DLR) (Lehner et al. 2000) from raw data provided by the European Space Agency (ESA). 1535 test imagettes classified by eye including four types of imagettes i. e. water, slick, ice and undefined inhomogeneous imagettes were applied to develop new classification parameters and are shown in Fig. 1. The newly-developed parameters are validated by nearly 1 million ERS-2 wave mode imagettes from 1 September 1998 to 30 November 2000.

HOAPS Wind Speed Data

The HOAPS wind speed data used in this study has a resolution of 0.25º×0.25º latitude-longitude grid. It is considered twice a day (0 UTC (0–12 UTC overpasses) and 12 UTC (12–24 UTC overpasses)). Each grid-cell contains the average of data from the satellite that passed this grid box closest to 12 and 24 UTC, respectively. The time range of HOAPS data used in this article is also from 1 September 1998 to 30
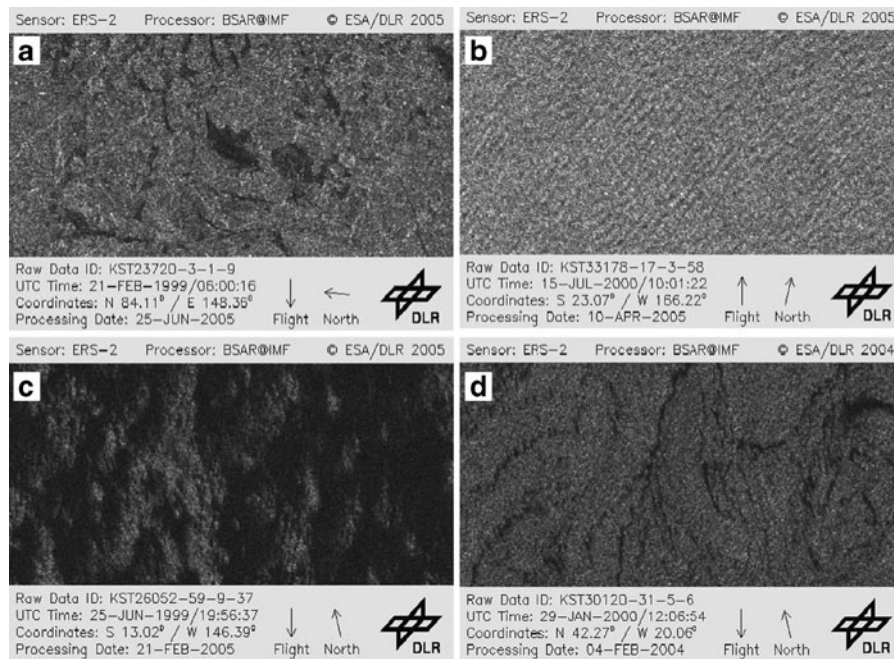
Fig. 1 Four types of imagettes: (**a**) ice, (**b**) water, (**c**) undefined, and (**d**) slick

November 2000. The HOAPS data have been used to understand the underlying reasons of inhomogeneity in the SAR imagettes. Many natural or artificial factors could contaminate the SAR imagette over the ocean such as low wind speed, precipitation, oil spill, atmospheric fronts, bottom topographic effect, currents and sea ice above 50 º N and 50 º S etc. However, the low wind speed, precipitation and oil spill are usually the most likely reasons to contaminate the SAR imagette over open ocean (Brekke and Solberg 2005). The HOAPS wind data is derived from special sensor microwave/imager (SSM/I) passive microwave radiometers and it was considered as the long time series (1987–2008) and high spatial resolution's wind satellite observations. It will be used to statistically calculate the percentage of the low wind speed over every 3°×3° longitude/latitude grid boxes. Its high spatial resolution could provide more samples over 3°×3° longitude/latitude grid boxes than other lower spatial resolution datasets.

New Classification and Parameter Developing

The homogeneity test (called *Inhomo*) used by CWAVE is based on the standard spectral estimation theory developed by Schulz-Stellenfleth and Lehner (2004). For *Inhomo* test, every imagette has been divided into 32 subimagettes of about 1×1 km size, which were used to estimate the mean and variance of the periodograms. The expectation value of the homogeneity parameter θ (*Inhomo*) is defined as

$$\theta = \frac{\sum_k \frac{\overline{var}(P_k)}{\overline{mean}(P_k)}}{\sum_k \overline{mean}(P_k)}, \tag{1}$$

where $\overline{mean}$ and $\overline{var}$ are the standard estimators for the periodograms mean and variances. P_k is the subimagette's periodogram. For a perfectly homogeneous imagette, the homogeneity parameter θ should be 1.

When *Inhomo* test is applied to 804,300 ERS-2 wave mode imagette data sets in order to filter the inhomogeneous ones, 741,264 imagettes were correctly classified. However, the remaining 63,036 imagettes were incorrectly classified as homogeneous ones. One apparent reason of this miscalculation could be because of the retrieved parameters (such as wind speed, significant wave height or mean wave period) from these 63,036 imagettes, which were negative. For CWAVE,

if the input imagette is homogeneous, the retrieved parameters should not be negative. The percentage of misclassification is found to be approximately 7.84 %. Figure 1 shows three examples among these 63,036 imagettes which were not correctly classified. Figures 1(a), (c) and (d) were classified by *Inhomo* test as homogeneous imagettes. However, all of these three imagettes are inhomogeneous in nature, which represent ice and undefined reasons caused the inhomogeneity and slickness. In view of the above analysis, it is essential to develop a new parameter for better classification of imagettes.

The Scheme of Division of Imagette

In every wave mode imagette, there are 512 pixels in the range direction with the resolution of 20 m and 1024 pixels in the azimuth direction with the resolution of 10 m. In this scheme, 5 pixels are selected in the range direction and 10 pixels are selected in the azimuth direction in every sub-imagette; thus the size of sub-imagette is about 100 m×100 m, and there are 10404 sub-imagettes in one wave mode imagette.

Definition of New Parameters

Several new classification parameters were investigated in this article. The definitions of them are as following:

(a) CoVar: the variance of the intensity of every sub-imagette divided by the mean value of intensity as ordinate versus the mean NRCS of the whole imagette as abscissa; a separation function to distinguish the homogeneous imagettes from inhomogeneous ones will be derived using the least squares fitting method.

(b) Min: The Minimum normalized radar cross section (NRCS) of sub-imagette as ordinate versus the mean NRCS of the whole imagette as abscissa; a separation function to distinguish the homogeneous imagettes from inhomogeneous ones will be derived using the least squares fitting method.

(c) Max: The Maximum NRCS of sub-imagette as ordinate versus the mean NRCS of the whole imagette as abscissa; a separation function also will be derived using the least squares fitting method.

(d) Percentile (PC): Figure 2 shows the sketch map of the definition of PC. The calculation process of PC can be seen from Eqs. 2–5. Firstly, the standard deviation δ could be calculated from the intensity of every pixel in an imagette (Eq. 2). Then, the mean intensity of the whole imagette ($\bar{I}$) will be calculated from Eq. 3. Consequently, - η can be defined as given in Eq. 4, which acts as a reference value of the pixel's intensity. It is assumed that 'n' is the number where the pixel's intensity is larger than η and 'N' is the total pixel number of the imagette. So the significance of PC is the percentage of the pixel's intensity which is larger than η (Eq. 4).

$$\delta = std(I) \tag{2}$$

$$\bar{I} = <I> \tag{3}$$

$$\eta = \bar{I} + 2\delta \tag{4}$$

$$PC = \frac{n}{N} * 100\% \tag{5}$$

A figure will be plotted using PC as ordinate and the mean NRCS of the whole imagette as abscissa. Similarly, a separation function will be derived using the least squares fitting method.
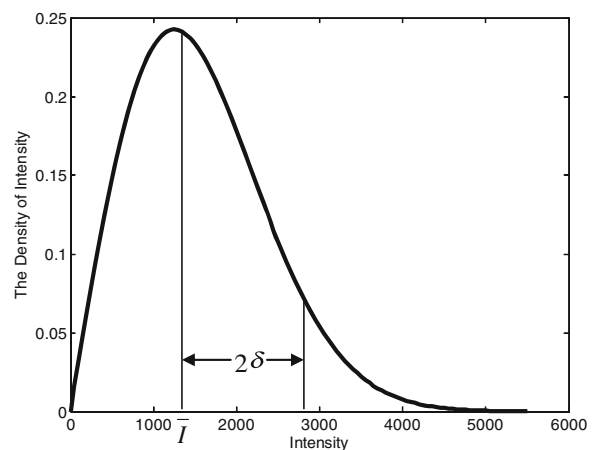

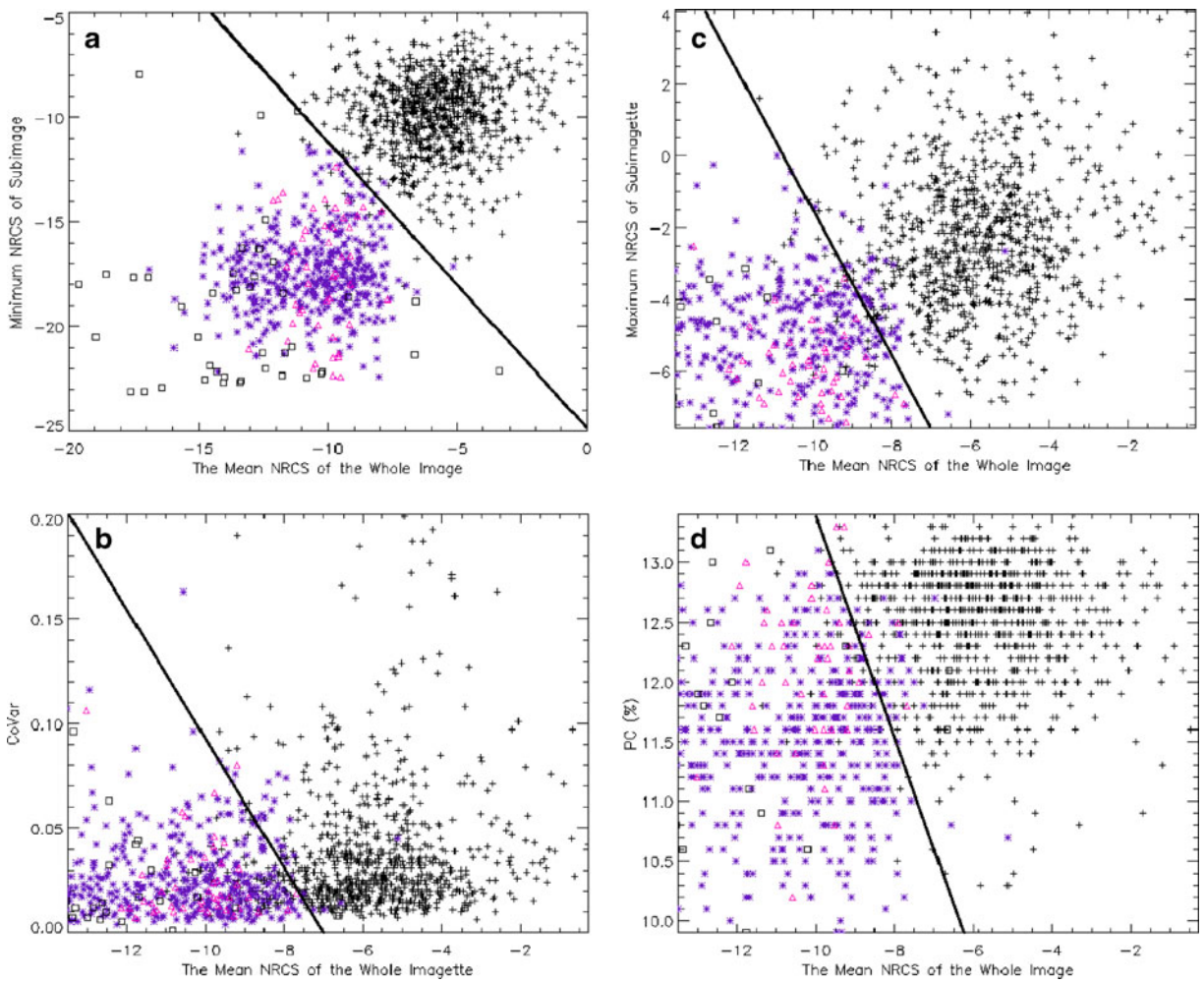**Fig. 2** The sketch map of the definition of Percentile

Fig. 3 (**a**–**b**): Results of different parameters using the test data: (**a**) Minimum NRCS of sub-imagette (Min) and (**b**) CoVar. Here, x-axis represents the mean NRCS of the whole imagette. The symbols '+', '*', 'Δ' and '□' represent water, ice, slick and undefined categories respectively. The line was fitted by least square method to separate the homogeneous water imagettes from other inhomogeneous ones including ice, slick and undefined inhomogeneous imgettes (**c**–**d**): Results of different parameters using the test data: (**c**) Maximum NRCS of sub-imagette (Max) and (**d**) Percentile (PC). Here, x-axis represents the mean NRCS of the whole imagette. The symbols '+', '*', 'Δ' and '□' represent water, ice, slick and undefined categories respectively. The line was fitted by least square method to separate the homogeneous water imagettes from other inhomogeneous ones including ice, slick and undefined inhomogeneous imgettes

Results and Discussion

The new parameters defined in Definition of new parameters sub-section are applied to the 1535 test

Table 1 The number of misclassifications (TNoM) for Min, CoVar, Max, PC and *Inhomo*

Parameter	Min	CoVar	Max	PC	*Inhomo*
TNoM	15	71	55	50	118

imagettes and the best one, which is the parameter of the least number of misclassifications, is chosen for further application and analysis.

Figure 3 shows the results of the different new parameters applied to the 1535 test imagettes and the separation function lines are fitted for every new classification parameter by least square method to classify the homogeneous water imagettes from other inhomogeneous ones including ice, slick and undefined inhomogeneous imagettes. The black plus symbols (+) representing imagettes obtained over ocean water,

Table 2 The number of misclassifications (TNoM) for *Inhomo* under varied threshold values

Inhomo	1.03	1.04	1.05	1.06	1.07	1.08	1.09	1.10	1.11
TNoM	128	125	123	121	118	122	123	125	126

which indicate the homogeneous ones, could be used for CWAVE. The purple star symbols (*) representing imagettes obtained over ice, the pink triangle symbols (△) for imagettes with slick and the black square ones (□) for undefined inhomogeneous imagettes indicate that the unclear reason causes the inhomogeneity. The number of misclassifications (TNoM) for every parameter including Min, CoVar, Max, PC and *Inhomo* is listed in Table 1. The TNoM for Min, CoVar, Max and PC are calculated from Fig. 3, and the TNoM for Inhomo was calculated by eye when the test imagettes datasets are prepared. It can be seen that the TNoM of Min is the least, which is only 15. The TNoMs of the four new parameters are much less than that of *Inhomo*. We also give a list of the TNoMs of *Inhomo*

under varied threshold values in Table 2. Currently, the threshold value of *Inhomo* used in CWAVE is 1.07 (Schulz-Stellenfleth et al. 2007), which is proved here that the threshold value of 1.07 is the best because both increase and decrease of the threshold value from 1.07 lead to a larger number of TNoM. When increasing the threshold value from 1.07, more inhomogeneous imagettes were misclassified into homogeneous ones, and when decreasing the threshold value from 1.07, more homogeneous imagettes were misclassified into inhomogeneous ones. Therefore, based on the statistical analysis and comparisons above, 'Min' should be chosen as the new standard classification parameter for further applications. After least squares fitting, the function for 'Min' $y=\tan(126°)x−24.9$, which approximates $y=−1.376x−24.9$, can be obtained to separate the homogeneous and inhomogeneous imagettes, where y is the minimum NRCS of sub-imagttes and x is the mean NRCS of the whole imagette. This separation function will be applied to the 2 years imagettes to distinguish the homogeneous

Fig. 4 The global distribution of inhomogeneous imagettes with 3°×3° longitude/latitude grid boxes from (**a**) new classification parameter Min and (**b**) *Inhomo* parameter
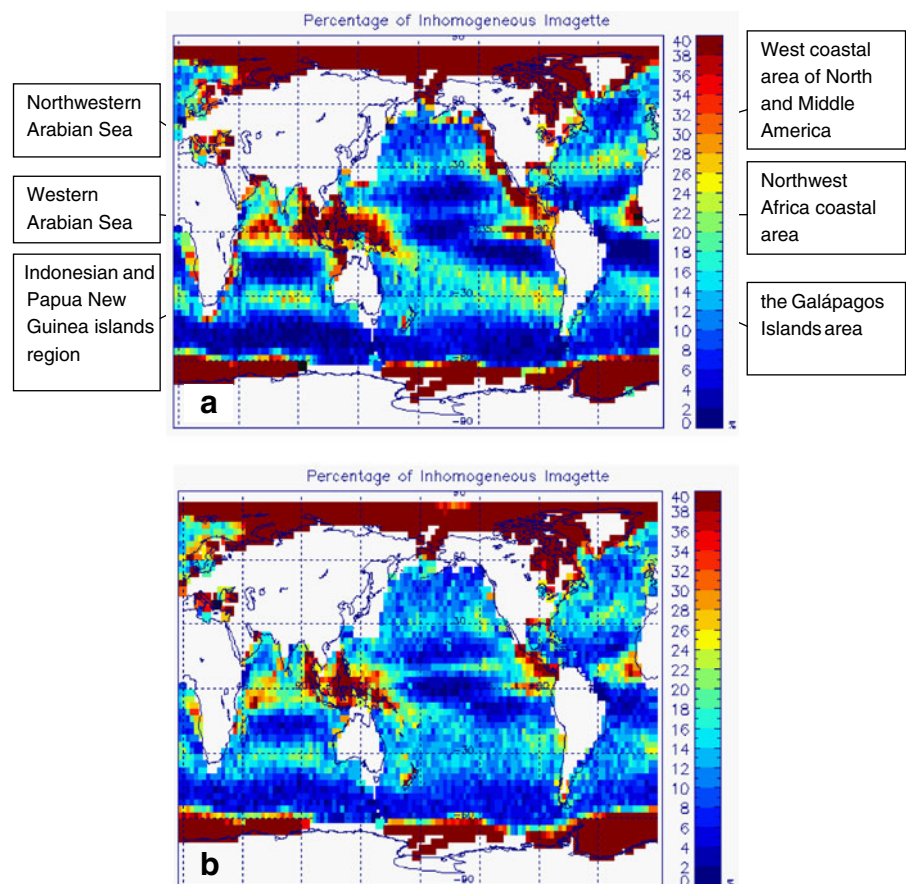
imagettes from inhomogeneous ones as a new classification parameter-Min.

The best new classification parameter (Min) and 'Inhomo' are applied to the 2 years' imagettes (about 1 million) of ERS-2 wave mode to compare their performance. All of the imagettes were obtained over ocean area. The 3°×3° latitude-longitude boxes over the global ocean were defined to statistically analyze the percentage of the inhomogeneous imagettes within each box. The global distributions of the percentage of the inhomogeneous imagettes using the parameter 'Min' (Fig. 4a) and 'Inhomo' (Fig. 4b) are shown in Fig. 4. In order to clearly present the difference of the

inhomogeneous distribution, the maximum percentage of inhomogeneity is set to 40 %. Both figures (Figs. 4a and b) show that the high percentage of inhomogeneous areas except the polar ice area locate in the ocean area of Indonesian and Papua New Guinea islands region, the west coastal area of north and Middle America, the western and northwestern Arabian Sea, the Galápagos Islands area and the coastal area of northwest Africa. However, there exist differences between the distribution of the new parameter 'Min' and the old one 'Inhomo'. In all of the large inhomogeneous regions, the areas of inhomogeneity calculated by 'Min' are a little larger than that

Fig. 5 The global distribution of inhomogeneous imagettes with 3°×3° longitude/latitude grid boxes for the percentage greater than 40 % which calculated from (a) new classification parameter (Min) and (b) Inhomo parameter
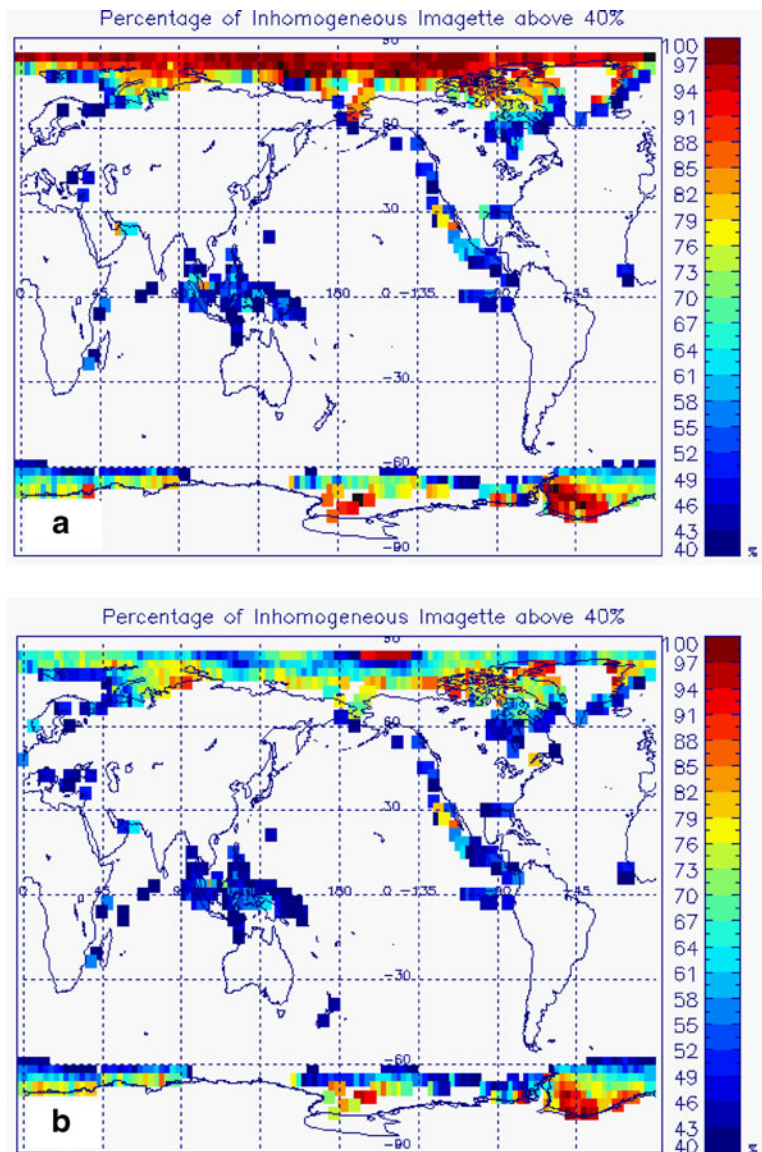
calculated by '*Inhomo*'. Also the color in the same area of inhomogeneity of '*Min*' shows much redder than that of '*Inhomo*'. These two features also exist in Fig. 5, which shows the global distribution of inhomogeneity greater than 40 %. Both of the Figs. 4 and 5 indicate that the parameter '*Min*' could filter more inhomogeneous imagettes than '*Inhomo*', which means that even when the '*Inhomo*' parameter's results are homogeneous, the parameter '*Min*' still could give the opposite judgment. Therefore, the parameter '*Min*' might be more powerful to filter the inhomogeneous imagettes than '*Inhomo*'.

The main reason of such strong inhomogeneous distribution in Figs. 4 and 5 is possibly due to the low wind speed as seen from Fig. 6. The high percentage HOAPS low wind speed (lower than 3 m/s) distributions in Fig. 6 agrees well with the inhomogeneous imagette distributions of Figs. 4 and 5. But the areas of the low wind speed are a little smaller than the inhomogeneous imagette areas. Under low wind speed condition, the SAR backscatter signal gets reduced; thus dark regions or spots will appear in the SAR images and the speckle level of the SAR image will be increased. This probably is the main reason of the consistent distribution of inhomogeneity of SAR imagette and low wind speed.

Conclusions

Synthetic aperture radar is one of the most applicable space-borne sensors for retrievals of ocean surface wind, ocean surface wave and internal wave, current fronts and ocean eddies. SAR images are also widely used to detect man-made illegal or accidental spills and natural seepage from oil deposits. In shallow waters, SAR imagery allows to infer the ocean bottom topography. All of these applications need to first distinguish the homogeneity property of the SAR image. In this study four new parameters are tested to better separate homogeneous imagettes from inhomogeneous ones. The '*Min*' parameter was chosen because of its best performance of separating the homogenous imagettes from inhomogeneous ones. The separation function of '*Min*' was fitted as $y=-1.376x-24.9$, where 'y' is the minimum NRCS of subimagettes and 'x' is the mean NRCS of the whole imagette. Comparisons between the new parameter '*Min*' and previous parameter '*Inhomo*' were done using both 1535 test imagettes and nearly 1 million imagettes collected for the period from September 1998 to November 2000. The comparisons imply that the new parameter '*Min*' classifies the property of the test imagettes much better than '*Inhomo*' and it is also more capable to filter inhomogeneous imagettes as compared to '*Inhomo*'. The new parameter '*Min*' can possibly be applied to CWAVE and is expected to better distinguish the homogeneity of the SAR imagette.

The inhomogeneous imagettes distribution agrees well with the low wind speed distribution from HOAPS datasets because low wind speed causes more speckle noise and nonlinear intensity inhomogeneity during SAR imaging. Under low wind speed the radar backscatter signal will be reduced and then dark regions or spots will appear in the SAR image, that is speckle noise.

A number of SAR missions are crucial for continuous SAR research. European radar satellites ERS-1,
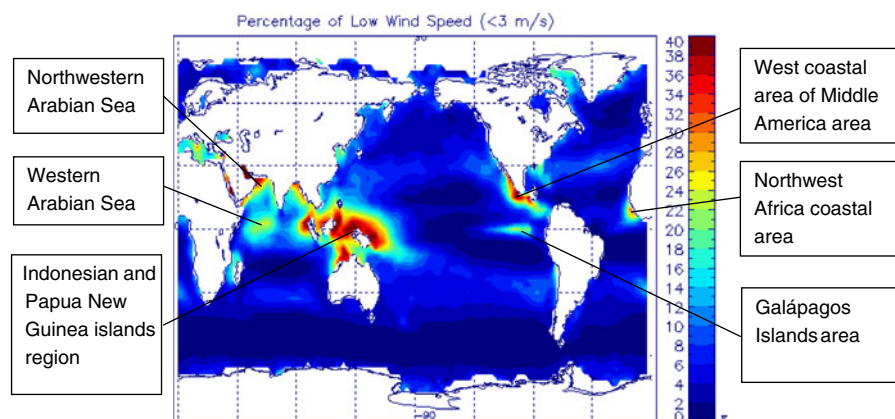

Fig. 6 The global distribution of low wind speed (lower than 3 m/s) with 3°×3° longitude/latitude grid boxes from HOAPS datasets

ERS-2, Envisat, TerraSAR-X and TanDEM-X provided valuable SAR images for this study. All of the SAR satellites provide wave mode SAR imagettes similar to the ones used in this paper. There is also a number of SAR missions planned. The new separation function (Min) can possibly be helpful in a wide range of applications in order to distinguish the homogeneity and inhomogeneity of SAR image.

References

Alpers, W., & Bruemmer, B. (1994). Atmospheric boundary layer rolls observed by the synthetic aperture radar aboard the ERS-1 satellite. *Journal of Geophysical Research, 99*, 12613–12621.

Brekke, C., & Solberg, A. H. S. (2005). Oil spill detection by satellite remote sensing. *Remote Sensing of Environment, 95*, 1–13.

Deb, S. K., Kishtawal, C. M., Pal, P. K., & Joshi, P. C. (2008). Impact of TMI SST on the simulation of heavy rainfall episode over Mumbai on 26th July 2005. *Monthly Weather Review, 136*(10), 3714–3741.

Deb, S. K., Bhowmick, S. A., Kumar, R., & Sarkar, A. (2009). Inter-comparison of numerical model generated surface winds with QuikSCAT winds over Indian Ocean. *Marine Geodesy, 32*(4), 391–408.

Deb, S. K., Kumar, P., Pal, P. K., & Joshi, P. C. (2011). Assimilation of INSAT data in simulation of recent tropical cyclone AILA. *International Journal of Remote Sensing, 32*(18), 5135–5155.

Hasselmann, K., Raney, R. K., Plant, W. J., Alpers, W., Shuchman, R. A., Lyzenga, D. R., Rufenach, C. L., & Tucker, M. J. (1985). Theory of synthetic aperture radar ocean imaging: a MARSEN view. *Journal of Geophysical Research, 90*, 4659–4686.

Horstmann, J., Schiller, H., Schulz-Stellenfleth, J., & Lehner, S. (2003). Global wind speed retrieval from SAR. *IEEE Transactions on Geoscience and Remote Sensing, 41*, 2277–2286.

Jaishwal, N., Kishtawal, C. M., & Pal, P. K. (2012). Cyclone intensity estimation using similarity of satellite IR images based on histogram matching approach. *Atmospheric Research, 118*, 215–221.

Jaishwal, N., Kishtawal, C. M., & Pal, P. K. (2013). Prediction of tropical cyclogenesis in North Indian Ocean using Oceansat-2 scatterometer (OSCAT) winds. *Meteorology and Atmospheric Physics, 119*, 137–149.

Lehner, S., Schulz-Stellenfleth, J., Schaettler, B., Breit, H., & Horstmann, J. (2000). Wind and wave measurements using complex ERS-2 SAR wave mode data. *IEEE Transactions on Geoscience and Remote Sensing, 38*(9), 2246–2257.

Lyzenga, D. R., Schuchman, R. A., & Lyden, J. D. (1985). SAR imaging of wave in water and ice: evidence for velocity bunching. *Journal of Geophysical Research, 90*, 1031–1036.

Marshall, J. L., Jung, J., Riishojgaard, L.-P., Lord, S., Derber, J., & Xiao, Y., et al. (2009). Satellite data assimilation, 5th WMO Workshop, 5–9 October, 2009 held at Melbourne, Australia.

Mitra, A. K., Kundu, P. K., & Giri, R. K. (2013). A quantitative analysis of KALPANA-1 derived water vapor winds and its impact on NWP model. *Meteorology and Atmospheric Physics, 120*, 29–44.

Panda, J., & Giri, R. K. (2012). A comprehensive study of surface and upper air characteristics over two stations on the west coast of India during the occurrence of a cyclonic storm. *Natural Hazards, 64*, 1055–1078.

Panda, J., Giri, R. K., Patel, K. H., Sharma, A. K., & Sharma, R. K. (2011). Impact of satellite derived winds and cumulus physics during the occurrence of the tropical cyclone Phyan. *Indian Journal of Science and Technology, 04*, 859–875.

Schulz-Stellenfleth, J., & Lehner, S. (2004). Measurement of 2-d sea surface elevation fields using complex synthetic aperture radar data. *IEEE Transactions on Geoscience and Remote Sensing, 42*, 1149–1160.

Schulz-Stellenfleth, J., Koenig, T., & Lehner, S. (2007). An empirical approach for the retrieval of integral ocean wave parameters from synthetic aperture radar data. *Journal of Geophysical Research, 112*, 3019–3033.